Journal of Power Sources 196 (2011) 10267–10279

Contents lists available at ScienceDirect

Journal of Power Sources

journal homepage: www.elsevier.com/locate/jpowsour

Comparison of discretization methods applied to the single-particle model of lithium-ion batteries

Aldo Romero-Becerril, Luis Alvarez-Icaza*

Instituto de Ingeniería, Universidad Nacional Autónoma de México, Ciudad Universitaria, 04510 Coyoacán, DF, Mexico

ARTICLE INFO

Article history:
Received 28 April 2011
Received in revised form 26 June 2011
Accepted 27 June 2011
Available online 2 July 2011

Keywords:
Lithium-ion battery
Electrochemical models
Single-particle model
Order reduction
Discretization

ABSTRACT

The single-particle model is a useful mathematical representation for state-of-charge observation, parameter identification and control of lithium-ion batteries. This model is a simplified electrochemical formulation where ionic intercalation, described as a diffusive process, is considered as the dominant dynamics. In the search for a more efficient numerical solution of the involved partial differential equations, many approximations have been reported. However, most of them are valid just under restricted operating conditions. In this paper, spatial semidiscretization is reintroduced as the precision of approximations could be arbitrarily chosen with this approach. Three discretization methods are applied in a classical fashion, evaluated and compared in both time and frequency domains: finite difference, finite element and differential quadrature. In addition, two commonly used low order approximations are tested against semidiscretization approximations. The best results are obtained with the differential quadrature method in its polynomial version. Two model truncation criteria are also explored, one is based on bandwidth selection and the other on residue analysis, where the first resulted to be more conservative. Finally, simulations of representative reduced order approximations of the single-particle model are compared against experimental data found in the literature.

1. Introduction

Due to a natural minimization trend, portable applications from cellular phones to hybrid electric vehicles require more efficient power sources such that energy could be stored in smaller and more lightweight devices. On the other hand, renewable resources like wind and solar energies are being used to complement or substitute traditional sources of electricity generation, helping to reduce the production of pollutants and the shortage of fossil fuels. However, as alternative energy sources depend on weather, electricity generated in excess should be stored and then released when demand is greater than production. Thereby, energy storage becomes crucial, making possible the existence of portable appliances and transforming renewable sources into reliable supplies.

Reviews about storage devices currently used in power systems could be found in [1,2]. Electrochemical batteries have represented the most popular alternative for more than one hundred years. Historical outlines about development of battery technologies, comparisons of materials and chemistries as well as specifications can be found in [3–5]. Batteries are in general low-power and high-energy storage devices; they can sustain plain charge or discharge conditions for long periods but are not well suited to manage power peaks. Dominant families of secondary (reversible or rechargeable) batteries are the lead-acid, nickel-based and lithium-ion (Li-Ion) systems. This last family represents the most promising technology, displacing nickel-based systems in the fields of electronic gadgets and medical implants, and is expected to be present in coming hybrid electric vehicles ([6–8]).

Li-Ion batteries posses the best performance features. For lead-acid batteries specific energy and power are 30 Wh kg^{-1} and 180 W kg^{-1}, whereas these specifications are 80–150 Wh kg^{-1} and 500–2000 W kg^{-1} for Li-Ion, and 100–150 Wh kg^{-1} and 50–250 W kg^{-1} for Li-Ion polymer batteries, respectively. Li-Ion systems do not present the memory effect, typical of the nickel-based family, have energy efficiencies of 90–100%, self discharge rates as low as 5% per month, can reach more than 1500 full charge–discharge cycles and have an open circuit potential around 3.7 V [2]. Although Li-Ion batteries have low environmental impact, many challenges are being faced in regard to materials and manufacturing processes to make this technology sustainable. Research about organic compounds, nanomaterials and lithium alternatives like aluminum and magnesium are being strongly impelled [9].

Mathematical models of batteries are combinations of static and/or dynamic relationships that set a correspondence between current and voltage at battery terminals (impedance), the only two measurable variables. Modeling is often intended to on-line estimation of non-measurable variables as the state-of-charge and

* Corresponding author. Tel.: +52 56233682; fax: +52 56233681.
E-mail addresses: aromerob@iingen.unam.mx, aldo.romerob@gmail.com (A. Romero-Becerril), alvar@pumas.iingen.unam.mx (L. Alvarez-Icaza).

0378-7753/$ – see front matter © 2011 Elsevier B.V. All rights reserved.
doi:10.1016/j.jpowsour.2011.06.091

the state-of-health (aging), as well as impedance identification. Other important objective is off-line battery simulation for design. Simulations make it possible the improvement of materials and optimization without actual manufacturing, reducing development time and costs [3].

Li-Ion battery models are in general of two types: equivalent circuits and electrochemical models. The first are very popular, being intuitive for people familiar with analysis of electric networks. There is a wide variety of them and are mainly used for impedance identification. Simple circuits, as the embedded in the Advanced Vehicle Simulator (ADVISOR) of the US National Renewable Energy Laboratory [10], or those reported in [11,12], are extensively used in practice, but more elaborated versions as [13–15] are also available. For these models, constitutive relationships of elements are complicated heuristic functions of state-of-charge (SOC) and temperature, and their use for analysis results difficult. SOC is the fundamental variable for battery control. Nevertheless, when equivalent circuits are used, SOC is estimated through numerical integration of the applied current (Coulomb counting), a not very accurate even robust method which drives to conservative power and energy management algorithms.

Electrochemical models were originally thought for battery design and optimization as they offer a better illustration about cell functioning and limitations. The formulation is based on physical and chemical principles, resulting in sets of coupled partial differential and algebraic equations. This approach allows accurate calculations of the spatial and temporal evolution of internal variables. Basic electrochemical models stated for charge–discharge prediction of Li-Ion cells with two porous electrodes, the systems currently used for power applications, can be found in [16–19], whereas a more formal reformulation is shown in [20]. Addition of further phenomena to the basic models like temperature changes, electric double-layer capacitance effect, battery aging and porosity variation are explored in [21–24], for example.

Obtaining rigorous numerical solutions of electrochemical models is time consuming and requires substantial computational resources. Equations are strongly coupled and this worsens as supplementary phenomena are appended. Even though, because of their physical meaning, high accuracy and more realistic SOC predictions, many efforts are being carried out to find appropriate simplifications and reduced order approximations that allow electrochemical models to be useful for on-line estimation and identification; see for example [25–33]. Depending on the application requirements, the first step is to define which dynamics are of interest, for example, concentration of lithium ions in the solid state, concentration of electrolyte in the electrolytic solution, the effect of double layer capacitance, cell aging, temperature changes or any combination. Then, the other dynamics could be either neglected or supposed static, driving to simpler models. As most of the phenomena involved in the operation of a lithium-ion cell are described by distributed parameter equations, simplified models can contain infinite order equations that should be efficiently numerically solved for on-line implementation.

In this paper, the single-particle model is studied as it constitutes a useful mathematical representation for state-of-charge observation, parameter identification and control of lithium-ion batteries. This model is a simplified electrochemical formulation where ionic intercalation, described as a diffusive process, is considered as the dominant dynamics. Such phenomenon is directly related to the SOC of the cell and voltage variations at the cell terminals. The other dynamics, referred above, are neglected because they have a weaker influence on the relationship between input current and output voltage. In particular, changes in temperature are ignored as the focus in this paper is on studying the effect of continuous charging–discharging cycles when a steady sate temperature has been reached.

The state equation of the single-particle electrochemical model is studied with the goal of finding reduced order approximations that represent adequately the battery main dynamics for some given operation conditions. Spatial semidiscretization approach is reintroduced for order reduction and three discretization methods, combined with four distributions of discretization points, are applied in a classical fashion: finite difference, finite element and differential quadrature. Because of their recurrent appearance in the literature, dynamical approximations based on second and fourth order polynomials are also evaluated and compared against semidiscretization approximations. Additionally, two order selection or truncation criteria, suggested but not explored in the literature, are discussed and contrasted. The first, more conservative, consists on selecting the bandwidth of the approximation such that it covers at least the major part of the energy spectrum of some proposed test signal. The second criterion is more relaxed and is based on a residue analysis of the convolution between the state equation and the test signal, driving to more practical results.

Approximations are first evaluated in the time domain to have a preliminary surmise about which is more accurate in comparison to a base solution. In this case, the test signal consists on a rectangular pulse followed by a relaxation time, whose duration is such that allows to observe the whole transient response under forced as well as under free excitation. Then, the frequency response of approximations is compared against that of an analytic transfer function related to the state equation in order to confirm the results obtained in the time domain tests. Finally, representative cases of all considered approximations are applied to the single-particle model and their response to the test signal specified in the FreedomCAR manual [34] is compared against experimental data extracted from [35]. Results indicate that differential quadrature approximations are the best and that low order polynomial-based approximations, commonly found in the literature, fail for pulsating operation conditions.

2. Single-particle electrochemical model

The considered Li-Ion cell, presented in [19], is one of 72 units taking part of a 6 Ah and 276 V pack designed for power assistance in hybrid electric vehicles. Secondary Li-Ion cells consist of three main components: negative electrode, separator and positive electrode. Electrodes are made of porous materials with insertions of lithium and inert conductive particles; carbon composites are used for the negative and metal oxides for the positive electrode. Separator is also a porous but electronically non-conductive matrix placed between the electrodes. Pores inside the three elements are filled with an electrolyte solution based on a lithium salt, setting up a ionic path all along the cell.

During discharge, lithium ions (Li^+) inside the active material of the negative electrode diffuse towards the boundary between solid and solution phases, and react (deintercalation). Once in the electrolyte, ions travel to the positive electrode where a corresponding reaction takes place (intercalation), but now ions diffuse from the interphase inside the solid phase. To keep an electric balance, electrons are delivered from the negative electrode and received in the positive, flowing through an external circuit as a usable current; an inverse and complementary process occurs when charging.

Electrochemical models of Li-Ion cells are based on the porous electrode theory [36], that states that porous electrodes could be treated as two overlapped phases. Because of the complexity of pores geometry, distribution of variables is analyzed just in the longitudinal dimension x that goes along the three elements of the cell. Major variables, as electrostatic potential in both phases, concentration of Li^+ in the solid matrix, concentration of electrolyte in the solution and ionic flux in the interphase depend on

both time and position x. The solid phase is modeled as a set of regular forms, usually spheres of the same radius. Lithium concentration in solid phase also depends on r, considered as a second pseudo-dimension, representing the position along the radius of a representative sphere of each electrode.

From simulations reported in [19,29,35] of the cell in study, it is observed that ionic flux in the solid-solution interphase, as well as concentration of Li^+ in the solid phase, become nearly independent of position x along electrodes very fast after the beginning of discharge. Furthermore, if these two variables are always considered independent of position x, the result is a decoupled model where lithium diffusion in the solid phase (intercalation and deintercalation) represents the dominant dynamics in the current–voltage relationship of the cell. In this case, electrolyte concentration in the solution is assumed constant, which drives to a simplification known as the single-particle electrochemical model. Such model was first introduced for nickel-metal hydride (NiMH) cells [37], then extended for Li-Ion batteries [26] and has been used for SOC estimation in works as [38–40]. Results of a deduction similar to that followed in [39] are summarized below and a more formal approach can be found in [20].

In the single particle model, lithium-ion diffusion in the solid phase is studied by means of one representative particle for each electrode. This phenomenon is described by the radial diffusion equation

$$\frac{\partial c}{\partial t} = D\frac{1}{r^2}\frac{\partial}{\partial r}\left(r^2\frac{\partial c}{\partial r}\right) \tag{1}$$

with boundary conditions

$$\left.\frac{\partial c}{\partial r}\right|_{r=0} = 0 \quad \text{and} \quad \left.\frac{\partial c}{\partial r}\right|_{r=R} = \frac{-j_n}{D}, \tag{2}$$

where $c = c(t, r)$ is the concentration of lithium ions inside the representative particle of the related electrode, D is the diffusivity constant of Li^+ in the solid phase, r is the position along the radius of the representative particle and R is the total radius of the particle. $j_n = j_n(t)$ is the normal ion flux in the solid-solution boundary, averaged along the associated electrode (see [39]) such that it is independent of position x and proportional to the applied current $I(t)$,

$$j_{n,p} = \frac{-I}{a_p\mathcal{F}\delta_p A} \quad \text{and} \quad j_{n,n} = \frac{I}{a_n\mathcal{F}\delta_n A} \tag{3}$$

for positive and negative electrodes, respectively. δ is the electrode thickness, A is the sectional area of the cell, $\mathcal{F}$ is the Faraday's constant and a is the electrode specific contact area. When needed, subscripts p, n and sep are included to distinguish between positive, negative electrodes and separator.

Voltage in terminals V is the difference of solid phase potential ϕ_s at cell edges:

$$V = \phi_s|_{x=0} - \phi_s|_{x=L} - R_f I, \tag{4}$$

where R_f is the equivalent film resistance at solid-solution interphase of electrodes and $L = \delta_p + \delta_{sep} + \delta_n$. Averaging the cell variables along electrodes and separator, Eq. (4) is rewritten as

$$V = U_p(\theta_p) - U_n(\theta_n) + \eta_p - \eta_n + \phi_{e,p} - \phi_{e,n} - R_f I, \tag{5}$$

with overpotential defined as $\eta = \phi_s - \phi_e - U$ and ϕ_e the electrostatic potential in the solution. Stoichiometry $\theta = c|_{r=R}/c^{\max}$ is defined as the normalized concentration of Li^+ in the solid-phase, also known as the electrode state-of-charge (do not confuse with battery state-of-charge or SOC). Open circuit potential functions $U(\theta)$ of both electrodes, taken from [19], are shown in Appendix A as well. Usually, the process of electrolyte solution is ignored; in this case such assumption means that $\phi_{e,p} - \phi_{e,n} = 0$. Instead, ohmic losses due to solution-phase are calculated for the three elements in [39]. The consecutive addition of losses results in

$$\phi_{e,p} - \phi_{e,n} = -\left(\frac{\delta_p}{2\kappa_p} + \frac{\delta_{sep}}{\kappa_{sep}} + \frac{\delta_n}{2\kappa_n}\right)\frac{I}{A}, \tag{6}$$

where δ_{sep} is the separator thickness and κ, with the corresponding subscript, represents the effective conductivity of the electrolyte solution in each element.

In [39], overpotentials η_p and η_n are found from the non-linear Butler–Volmer reaction equation, resulting in an expression equivalent to

$$\eta_p - \eta_n = \frac{2\mathcal{RT}}{\mathcal{F}}\ln\left[\frac{(\mathcal{F}j_{n,p}/i_{0,p}) + \sqrt{(\mathcal{F}j_{n,p}/i_{0,p})^2 + 1}}{(\mathcal{F}j_{n,n}/i_{0,n}) + \sqrt{(\mathcal{F}j_{n,n}/i_{0,n})^2 + 1}}\right] \tag{7}$$

where i_0 is the exchange current density, $\mathcal{R}$ the ideal gas constant and $\mathcal{T}$ the absolute temperature. Alternatively, using the linearized Butler–Volmer equation

$$j_n = i_0\frac{(\alpha_a + \alpha_c)\eta}{\mathcal{RT}}, \tag{8}$$

with $\alpha_a = \alpha_c = 0.5$, the results is

$$\eta_p - \eta_n = \frac{\mathcal{RT}}{\mathcal{F}}\left(\frac{1}{a_p\delta_p i_{0,p}} - \frac{1}{a_n\delta_n i_{0,n}}\right)\frac{I}{A}. \tag{9}$$

Taking (9) instead of (7), voltage at terminals is finally

$$V = U_p(\theta_p) - U_n(\theta_n) - R_\Omega I, \tag{10}$$

with the total resistance R_Ω defined as

$$R_\Omega = \frac{1}{A}\left(\frac{\delta_p}{2\kappa_p} + \frac{\delta_{sep}}{\kappa_{sep}} + \frac{\delta_n}{2\kappa_n} - \frac{\mathcal{RT}}{a_p\delta_p i_{0,p}\mathcal{F}} + \frac{\mathcal{RT}}{a_n\delta_n i_{0,n}\mathcal{F}}\right) + R_f. \tag{11}$$

In summary, the single-particle electrochemical model is represented by Eqs. (1)–(3) and (10), where the applied current I is the input, the voltage V at terminals is the output signal and the state variables c_n and c_p correspond to concentration of Li^+ in both electrodes. Values of parameters, extracted from [29], are listed in Appendix B. For pulsating charge–discharge conditions around nominal current, assumption of uniform electrolyte concentration is acceptable in general. For long term constant charge or discharge regimes, or for high pulsating currents, it would be necessary to find limiting conditions of discharge time and/or current intensity to assure that the electrolyte solution along the cell will not run out of electrolyte in any place. The procedure proposed in [25] could be followed for this purpose.

3. Spatial semidiscretization approach

Spatial semidiscretization, also known as the method of lines, consists on approximating the state variable in a set of discrete points, arbitrarily located in the spatial domain, by means of a system of ordinary differential and algebraic equations. For simplicity, the state and position variables c and r are normalized against the maximum value $c^{\max}$ and the radius R of the representative particle, respectively. Then the state Eq. (1) is rewritten as

$$\frac{\partial\Theta}{\partial t} = K\frac{1}{\rho^2}\frac{\partial}{\partial\rho}\left(\rho^2\frac{\partial\Theta}{\partial\rho}\right) \tag{12}$$

and boundary conditions (2) take the form

$$\alpha(t) = \left.\frac{\partial\Theta}{\partial\rho}\right|_{\rho=0} = 0 \quad \text{and} \quad \beta(t) = \left.\frac{\partial\Theta}{\partial\rho}\right|_{\rho=1} = \frac{-Rj_n}{D}, \tag{13}$$

where $K = D/R^2$, $\Theta(t, \rho) = c(t, r/R)/c^{\max}$, $\rho = r/R$ and $\{\Theta, \rho\} \in [0, 1]$. Electrode state-of-charge, which is needed to evaluate the objective function (10), is then $\theta = \Theta(t, 1)$.

Applying the spatial semidiscretization approach, the diffusion problem (12) and (13) is approximated for each electrode by the system of linear ordinary differential equations

$$\frac{\mathrm{d}\boldsymbol{\Theta}}{\mathrm{d}t} = K\left(\mathbf{A}\boldsymbol{\Theta} + \mathbf{B}\beta\right), \tag{14}$$

over the whole set of points ρ_i, with $i = 1, 2, \ldots, N$, or just in a subset. Depending on the discretization method, a differential equation does not exist at specific points, usually the boundaries. This happens for the finite difference and the differential quadrature methods applied in a classical fashion. Electrode state-of-charge $\theta = \Theta(t, 1) = \Theta_N$, which lies in the outermost boundary, it is calculated as a linear combination of the elements of $\boldsymbol{\Theta}$ and the boundary condition β, such that

$$\theta = \mathbf{C}\boldsymbol{\Theta} + \mathbf{D}\beta. \tag{15}$$

The value of state variable at $\rho = 0$ is not of interest for the single-particle model. However, $\Theta(t, 0) = \Theta_1$ is needed for evaluations in time domain and could be calculated similarly to Θ_N.

Although $\Theta_N \in \boldsymbol{\Theta}$ for the finite element method, representation (15) is also valid for such discretization method. Matrices $\mathbf{A} \in \mathbb{R}^{q\times q}$, $\mathbf{B} \in \mathbb{R}^{q\times 1}$, $\mathbf{C} \in \mathbb{R}^{1\times q}$ and $\mathbf{D} \in \mathbb{R}$ are a result of discretization and their elements are different in general, depending on the related electrode, the discretization method and the number of points as well as their distribution. Matrices $\mathbf{B}$ and $\mathbf{D}$ are the second column of $\hat{\mathbf{B}} \in \mathbb{R}^{q\times 2}$ and $\hat{\mathbf{D}} \in \mathbb{R}^{1\times 2}$, respectively. The first column of $\hat{\mathbf{B}}$ and $\hat{\mathbf{D}}$ corresponds to the boundary condition α, which is out of the formulation due to its null influence. Index q, defined later for each discretization method, is the length of vector $\boldsymbol{\Theta}$ and also represents the order of the system of differential Eq. (14).[1] Thus, q_p is the order of the subsystem which approximates the diffusion equation associated to the positive electrode and q_n is similarly defined for the negative electrode.

According to the spatial semidiscretization approach, the complete single-particle electrochemical model is approximated by the system of ordinary differential and algebraic equations

$$\frac{\mathrm{d}}{\mathrm{d}t}\begin{bmatrix}\boldsymbol{\Theta}_p\\ \boldsymbol{\Theta}_n\end{bmatrix} = \begin{bmatrix}K_p\mathbf{A}_p & \mathbf{0}\\ \mathbf{0} & K_n\mathbf{A}_n\end{bmatrix}\begin{bmatrix}\boldsymbol{\Theta}_p\\ \boldsymbol{\Theta}_n\end{bmatrix} + \begin{bmatrix}-\mu_p\mathbf{B}_p\\ \mu_n\mathbf{B}_n\end{bmatrix} I, \tag{16}$$

$$\theta_p = \mathbf{C}_p\boldsymbol{\Theta}_p + \mathbf{D}_p I, \tag{17}$$

$$\theta_n = \mathbf{C}_n\boldsymbol{\Theta}_n + \mathbf{D}_n I, \tag{18}$$

$$V = U_p(\theta_p) - U_n(\theta_n) - R_\Omega I, \tag{19}$$

where $\mu = R/(Da\mathcal{F}\delta A)$. In (16), dynamics of positive and negative electrodes are put together and then the order of the complete approximated model is $Q = q_p + q_n$.

4. Discretization methods

Some approximations based on spatial semidiscretization for diffusion problem (1) and (2) have been reported. For example, a fifth order finite element approximation is proposed in [35] and the finite difference method is applied in [39]. Nevertheless, in neither of both works it is specified why to choose one or the other discretization method or how to determine the order of approximation. Thus, the aim of this work is to identify which one among three discretization methods, combined with four grids, offers the best trade off between low order and accuracy for the diffusion problem (12) and (13): finite difference, finite element and differential quadrature. In addition, two criteria for order selection are explored and compared. In these subsections, a brief overview of the considered discretization methods is presented. All of them are applied in a classical fashion.

4.1. Finite difference method (FD)

The three-point centered finite difference is maybe the most popular discretization method. In this case, for one dimension problems, derivatives of any order with respect to x of a function $f(x)$ are approximated throughout a grid by means of point operators, which depend on $f(x)$ evaluated in the point of interest x_i and the neighboring points x_{i-1} and x_{i+1}. Operators are derived by taking linear combinations of Taylor series of $f(x_{i-1})$, $f(x_i)$ and $f(x_{i+1})$ around x_i, as well as $\partial f(x_1)/\partial x$ and $\partial f(x_N)/\partial x$ when necessary. See [41,42] for more details and further FD schemes.

With the three-point centered FD method it is not possible to formulate differential equations at the boundary points $\rho_1 = 0$ and $\rho_N = 1$, then, state vector is $\boldsymbol{\Theta} = \left[\Theta_2\ \Theta_3 \cdots \Theta_{N-1}\right]^\top$ with $\Theta_i = \Theta|_{\rho_i}$ and $q = N - 2$. It is convenient to take the expanded form

$$\frac{\partial\Theta}{\partial t} = K\left(\frac{\partial^2\Theta}{\partial\rho^2} + \frac{2}{\rho}\frac{\partial\Theta}{\partial\rho}\right) \tag{20}$$

of Eq. (12), whose discretization with the introduction of boundary conditions results in

$$\frac{\mathrm{d}\Theta_i}{\mathrm{d}t} = K\begin{cases}\displaystyle\sum_{k=i}^{i+1}\left(b_{i,k} + \frac{2}{\rho_i}a_{i,k}\right)\Theta_k + c_1\alpha & \text{for}\quad i = 2,\\ \displaystyle\sum_{k=i-1}^{i+1}\left(b_{i,k} + \frac{2}{\rho_i}a_{i,k}\right)\Theta_k & \text{for}\quad i = 3, \ldots, N-2,\\ \displaystyle\sum_{k=i-1}^{i}\left(b_{i,k} + \frac{2}{\rho_i}a_{i,k}\right)\Theta_k + c_N\beta & \text{for}\quad i = N-1,\end{cases} \tag{21}$$

where N is the total number of points. State variable $\Theta(t, \rho)$ is approximated at boundaries $\rho = 0$ and $\rho = 1$ through the expressions

$$\Theta_1 = d_1\alpha + d_2\Theta_2 + d_3\Theta_3, \tag{22}$$

$$\Theta_N = d_{N-2}\Theta_{N-2} + d_{N-1}\Theta_{N-1} + d_N\beta, \tag{23}$$

that can be obtained from a combination of the first and second, and second and third lines of (21), respectively. Coefficients $a_{i,k}$ and $b_{i,k}$ are related to the first and second spatial derivative and, in addition to c_N and $d_\circ$, are explicitly calculated in function of discretization points as shown in Table 1, whereas c_1 is irrelevant here and in all cases as $\alpha = 0$. Once coefficients are known, (21) and (22) could be easily brought to matrix form (14) to (15).

4.2. Finite element method (FE)

This is also a well known discretization method and is widely used to simulate multidimensional problems with irregular geometries because of its easy numerical assembling. For one dimensional problems and taking the simplest formulation, the aim of the FE method is to approximate the profile of $f(x)$ by linear segments like

$$f(x) \approx \frac{x_{i+1} - x}{x_{i+1} - x_i}f(x_i) + \frac{x - x_i}{x_{i+1} - x_i}f(x_{i+1}), \tag{24}$$

where the factors of $f(x_i)$ and $f(x_{i+1})$ are called aspect functions. With this method it is possible to define ordinary differential equations in every point when Neumann type boundary conditions as (13)

[1] Unless stated otherwise, in this paper order always refers to the number of differential equations in the resulting system.

Table 1
Coefficients for the FD method.

i	Coefficients	
1	$d_2 = \frac{(\rho_3-\rho_1)^2}{(\rho_3-\rho_2)(\rho_3+\rho_2-2\rho_1)}$	$d_3 = \frac{-(\rho_2-\rho_1)^2}{(\rho_3-\rho_1)(\rho_3+\rho_2)}$
2	$b_{2,2} = \frac{-2}{(\rho_3-\rho_2)(\rho_3+\rho_2-2\rho_1)}$ $b_{2,3} = -b_{2,2}$	$a_{2,2} = \frac{-2(\rho_2-\rho_1)}{(\rho_3-\rho_2)(\rho_3+\rho_2-2\rho_1)}$ $a_{2,3} = -a_{2,2}$
3	$b_{i,i-1} = \frac{2}{(\rho_i-\rho_{i-1})(\rho_{i+1}-\rho_{i-1})}$	$a_{i,i-1} = \frac{-(\rho_{i+1}-\rho_i)}{(\rho_i-\rho_{i-1})(\rho_{i+1}-\rho_{i-1})}$
⋮	$b_{i,i} = \frac{-2}{(\rho_i-\rho_{i-1})(\rho_{i+1}-\rho_i)}$	$a_{i,i-1} = \frac{\rho_{i+1}-2\rho_i+\rho_{i-1}}{(\rho_i-\rho_{i-1})(\rho_{i+1}-\rho_i)}$
$N-2$	$b_{i,i+1} = \frac{2}{(\rho_{i+1}-\rho_i)(\rho_{i+1}-\rho_{i-1})}$	$a_{i,i+1} = \frac{\rho_i-\rho_{i-1}}{(\rho_{i+1}-\rho_i)(\rho_{i+1}-\rho_{i-1})}$
$N-1$	$b_{N-1,N-2} = \frac{2}{(\rho_{N-1}-\rho_{N-2})(2\rho_N-\rho_{N-1}-\rho_{N-2})}$	
	$a_{N-1,N-2} = \frac{-2(\rho_N-\rho_{N-1})}{(\rho_{N-1}-\rho_{N-2})(2\rho_N-\rho_{N-1}-\rho_{N-2})}$	
	$b_{N-1,N-1} = -b_{N-1,N-2}$	$a_{N-1,N-1} = -a_{N-1,N-2}$
	$c_N = \frac{2+\rho_{N-1}-\rho_{N-2}}{2\rho_N-\rho_{N-1}-\rho_{N-2}}$	
N	$d_{N-2} = \frac{-(\rho_N-\rho_{N-1})^2}{(\rho_{N-1}-\rho_{N-2})(2\rho_N-\rho_{N-1}-\rho_{N-2})}$	
	$d_{N-1} = \frac{(\rho_N-\rho_{N-2})^2}{(\rho_{N-1}-\rho_{N-2})(2\rho_N-\rho_{N-1}-\rho_{N-2})}$	
	$d_N = \frac{(\rho_N-\rho_{N-1})(\rho_N-\rho_{N-2})}{(2\rho_N-\rho_{N-1}-\rho_{N-2})}$	

are given. In this case $\boldsymbol{\Theta} = \left[\Theta_1\ \Theta_2 \cdots \Theta_N\right]^\top$ and $q = N$. The diffusion problem (12) and (13) is approximated by

$$\frac{\mathrm{d}\Theta_i}{\mathrm{d}t} = K \begin{cases} \displaystyle\sum_{k=i}^{i+1} b_{i,k}\Theta_k + c_1\alpha & \text{for} \quad i = 1, \\ \displaystyle\sum_{k=i-1}^{i+1} b_{i,k}\Theta_k & \text{for} \quad i = 2, \ldots, N-1, \\ \displaystyle\sum_{k=i-1}^{i} b_{i,k}\Theta_k + c_N\beta & \text{for} \quad i = N-1. \end{cases} \tag{25}$$

Coefficients $b_{i,k}$ and c_N, shown in Table 2, are found by solving the error integral function

$$R_i = -\int_{\rho_{i-1}}^{\rho_{i+1}} W_i \left[K\frac{1}{\rho^2}\frac{\partial}{\partial\rho}\left(\rho^2\frac{\partial\Theta}{\partial\rho}\right) - \frac{\partial\Theta}{\partial t}\right] \tag{26}$$

for each grid point, including the boundaries. The integral is evaluated in two parts, one for each element associated to ρ_i, and taking the appropriate aspect function as weight W_i (Galerkin's method). For the temporal derivative of Θ, the *lumped formulation* has been considered, which consists on assuming the term $\partial\Theta/\partial t$ as a constant for the point ρ_i of interest and half of each of the two adjacent elements see [43]. The *consistent formulation* has been discarded because of its probed tendency to produce oscillations.

Table 2
Coefficients for the FE method.

i	Coefficients	
1	$b_{1,1} = \frac{\rho_1^3-\rho_2^3}{\left[\frac{1}{8}(\rho_1+\rho_2)^3-\rho_1^3\right](\rho_1-\rho_2)^2}$	$b_{1,2} = -b_{1,1}$
2	$b_{i,i-1} = \frac{-8(\rho_{i-1}^3-\rho_i^3)}{\left[-(\rho_{i-1}-\rho_i)^3+(\rho_i-\rho_{i+1})^3\right](\rho_{i-1}-\rho_i)^2}$	
⋮	$b_{i,i} = \frac{8}{\left[-(\rho_{i-1}-\rho_i)^3+(\rho_i-\rho_{i+1})^3\right](\rho_{i-1}-\rho_i)^2}\left[\frac{\rho_{i-1}^3-\rho_i^3}{(\rho_{i-1}-\rho_i)^2}+\frac{\rho_i^3-\rho_{i+1}^3}{(\rho_i-\rho_{i+1})^2}\right]$	
$N-1$	$b_{i,i+1} = \frac{-8(\rho_i^3-\rho_{i+1}^3)}{\left[-(\rho_{i-1}-\rho_i)^3+(\rho_i-\rho_{i+1})^3\right](\rho_i+\rho_{i+1})^2}$	
N	$b_{N,N-1} = \frac{-(\rho_{N-1}^3-\rho_N^3)}{\left[\rho_N^3-\frac{1}{8}(\rho_{N-1}-\rho_N)^3\right](\rho_{N-1}-\rho_N)^2}$	$b_{N,N} = -b_{N,N-1}$
	$c_N = \frac{\rho_N^2}{\frac{1}{3}\rho_N^3-\frac{1}{24}(\rho_{N-1}+\rho_N)^3}$	

4.3. Differential quadrature method (DQ)

In contrast to both methods described before, differential quadrature is less popular despite its generality, easy implementation and good approximations. It is based in the assumption that some smooth function $f(x)$ can be approximated by a polynomial like $\sum_{k=1}^{N} C_k x^{k-1}$ or a trigonometric series of form $A_0 + \sum_{k=1}^{N/2}(A_k\cos kx + B_k\sin kx)$. The first case is called polynomial differential quadrature (PDQ) and the second case corresponds to the Fourier-based differential quadrature (FDQ). As a consequence of this formulation, any differential operator $\partial^n f(x)/\partial x^n$ of order n is approximated at x_i by linear combinations of the functional values of $f(x)$ at every discretization point [44], not just at adjacent points as for FD and FE.

When applied in a classical way, no differential equations can be stated for the boundary points with the DQ method (see [45] for imposition of boundary conditions at interior points), and $\boldsymbol{\Theta}$ and q are the same that for FD. In general, the expanded form (20) of (12) is discretized as

$$\frac{\mathrm{d}\Theta_i}{\mathrm{d}t} = K\left[\sum_{k=2}^{N-1}\left(\hat{b}_{i,k} + \frac{2}{\rho_i}\hat{a}_{i,k}\right)\Theta_k + c_i\beta\right] \quad \text{for} \quad i = 2, \ldots, N-1. \tag{27}$$

It should be underlined that there is a coefficient c_i for each point because β has a direct influence in every location.

Due to imposition of boundary conditions, coefficients $\hat{a}_{i,k}$, $\hat{b}_{i,k}$ and c_i are indirectly calculated in function of the discretization points ρ_i through the more elemental coefficients $a_{i,k}$ and $b_{i,k}$, related to the first and second derivative as well, such that

$$\hat{b}_{i,k} = b_{i,k} + P\left[a_{1,k}(b_{i,N}a_{N,1} - b_{i,1}a_{N,N}) + a_{N,k}(b_{i,1}a_{1,N} - b_{i,N}a_{1,1})\right], \tag{28}$$

$$\hat{a}_{i,k} = a_{i,k} + P\left[a_{1,k}(a_{i,N}a_{N,1} - a_{i,1}a_{N,N}) + a_{N,k}(a_{i,1}a_{1,N} - a_{i,N}a_{1,1})\right], \tag{29}$$

$$c_i = P\left[b_{i,N}a_{1,1} - b_{i,1}a_{1,N} + \frac{2}{\rho_i}(a_{i,N}a_{1,1} - b_{i,1}a_{1,N})\right], \tag{30}$$

where $P = (a_{1,1}a_{N,N} - a_{1,N}a_{N,1})^{-1}$. At boundaries, state variable $\Theta(t, \rho)$ is approximated by the equations

$$\Theta_1 = P\left[-a_{1,N}\beta + \sum_{k=2}^{N-1}(a_{1,N}a_{N,k} - a_{N,N}a_{1,k})\Theta_k\right], \tag{31}$$

$$\Theta_N = P\left[-a_{N,1}\beta + \sum_{k=2}^{N-1}(a_{N,1}a_{1,k} - a_{1,1}a_{N,k})\Theta_k\right]. \tag{32}$$

In the case of PDQ, coefficients $a_{i,k}$ are

$$a_{i,k} = \begin{cases} \dfrac{\displaystyle\prod_{j=1, j\neq i}^{N}(\rho_i - \rho_j)}{(\rho_i - \rho_k)\displaystyle\prod_{j=1, j\neq k}^{N}(\rho_k - \rho_j)} & \text{for} \quad i \neq k, \quad \{i, k\} = 1, \ldots, N \\ -\displaystyle\sum_{k=1, k\neq i}^{N} a_{i,k} & \text{for} \quad i = k, \quad \{i, k\} = 1, \ldots, N. \end{cases} \tag{33}$$

Likewise, for FDQ

$$a_{i,k} = \begin{cases} \dfrac{\displaystyle\prod_{j=1, j\neq i}^{N} \sin((\rho_i - \rho_j)/2)}{\sin((\rho_i - \rho_k)/2)\displaystyle\prod_{j=1, j\neq k}^{N} \sin((\rho_k - \rho_j)/2)} & \text{for} \quad i \neq k, \quad \{i, k\} = 1, \ldots, N \\ -\displaystyle\sum_{k=1, k\neq i}^{N} a_{i,k} & \text{for} \quad i = k, \quad \{i, k\} = 1, \ldots, N. \end{cases} \tag{34}$$

In both cases, if coefficients $a_{i,k}$ are the elements of a matrix $\mathbf{W}^{(1)}$, then $b_{i,k}$ is an element of matrix $\mathbf{W}^{(2)} = \left[\mathbf{W}^{(1)}\right]^2$.

4.4. Distributions of discretization points

Accuracy of discretization methods depends on a great extent on the location of discretization points. For this reason, four grids are tested along with the discretization methods.

Uniform distribution (UD): Discretization points are evenly placed throughout the domain of interest.

Chebyshev–Gauss–Lobatto distribution (CGL): points become closer towards the domain boundaries according to

$$\rho_i = \frac{1}{2}\left(1 - \cos\frac{i-1}{N-1}\pi\right) \quad \text{for} \quad i = 1, \ldots, N. \tag{35}$$

Roots of shifted Legendre polynomials (RLP): Legendre associated polynomials are deducted from the recursive formula

$$P_{n+1}(\bar{\rho}) = \frac{(2n+1)\bar{\rho}P_n(\bar{\rho}) - nP_{n-1}(\bar{\rho})}{n+1}, \tag{36}$$

with $P_0 = 1$ and $P_1 = \bar{\rho}$. Roots of such polynomials lie on $\bar{\rho} \in (-1, 1)$. After shifting the roots to the domain $\rho \in (0, 1)$ by means of the transformation $\bar{\rho} = 2\rho - 1$, and including the auxiliary points $\rho_1 = 0$ and $\rho_N = 1$, the elements of the resulting set could be used as discretization points.

Proportional distribution (PD): As stated in [43], results from FE method can be improved if the grid is tightened where changes in the variable of interest are more pronounced. For this grid, points become closer towards the boundary point $\rho = 1$ in a square proportion defined by

$$\rho_i = \sqrt{\frac{i-1}{N-1}}. \tag{37}$$

Such heuristic distribution is proposed because it is known that the state variable tends to have a parabolic profile in the spatial variable.

5. Order selection

The two order selection or truncation criteria suggested but not discussed in [30] are explored in this section. The first is based in the model bandwidth selection whereas, in the second, a residue analysis is carried out. In both cases, the supposition of a specific profile for the boundary condition $\beta(t)$, the input of each electrode subsystem, plays a key role. In particular, it is considered that the current profile used in [35], the FreedomCAR Hybrid Pulse Power Characterization (HPPC) [34], is applied to the Li-Ion cell. One cycle of that test signal consists on three constant stages: a 30 A and 18 s discharge pulse, an open-circuit (0 A) relaxation period of 32 s and, finally, a 22.5 A and 10 s charge pulse. Nevertheless, it is helpful first to study the case where β is a simple rectangular pulse as results are straightforward extended for every signal composed of rectangular pulses of any amplitude and duration.

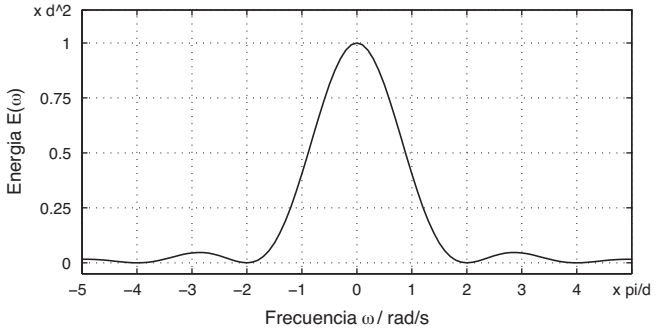

Fig. 1. Energy spectrum of a rectangular pulse.

5.1. Truncation by bandwidth selection

This criterion consists on choosing the order of the system such that its spectrum covers all or, at least, the major part of the bandwidth associated to a test signal. Supposing β is a rectangular pulse

$$\beta(t) = \begin{cases} 1 & \text{for} \quad t \in [0,\ d) \\ 0 & \text{for} \quad t \in [d,\ \infty), \end{cases} \tag{38}$$

of unitary amplitude and duration $d > 0$, it can be easily shown that its energy spectrum is given by

$$E(\omega) = \left|\hat{\beta}(\omega)\right|^2 = d^2 \mathrm{sinc}^2\left(\frac{\omega d}{2\pi}\right), \tag{39}$$

where $\hat{\beta}(\omega)$ is the Fourier transformation of (38) and $\mathrm{sinc}(x) = \sin(\pi x)/\pi x$. From Fig. 1 it is observed that the first zero of (39) occurs at $\omega = \pm 2\pi/d$. Furthermore, taking the integral of (39) over the interval $\omega \in [-2\pi/d,\ 2\pi/d]$, it is concluded that ~90% of energy is contained in the bandwidth $\omega \in [0,\ 2\pi/d]$.

The characteristic values λ_m of the diffusion problem (12) and (13) could be found solving the associated regular Sturm–Liouville problem for the homogeneous case [46]. All are real and nonnegative [35] such that

$$\lambda_m = \begin{cases} 0 & \text{for} \quad m = 1 \\ y_m > 0 | y_m = \tan y_m & \text{for} \quad m > 1, \end{cases} \tag{40}$$

and the transient response of the solution $\Theta(t,\ \rho)$ of (12) and (13) to any input β will be determined by modes of the form $\exp(p_m t)$, with $p_m = -K\lambda_m^2$, for $m = 1, 2, \ldots$ Let p_q be the constant of the faster mode. Then, with this truncation criterion, it should be satisfied that $|p_q| \geq 2\pi/d$ to ensure that the reduced order model spectrum covers the bandwidth where most of energy of the input signal is concentrated, which implies that

$$\lambda_q^2 \geq \frac{2\pi}{Kd}. \tag{41}$$

When β consists of more than one pulse, it is enough just to study that of minimum duration because its 90%-energy bandwidth actually covers more than that for longer duration pulses.

5.2. Truncation by residue analysis

The output function (10) or (19) depends on the concentration of Li^+ evaluated just at the surface of the representative particle of each electrode, namely, $\theta = \Theta(t,\ 1)$. If variables β and $\Theta(t,\ 1)$ are defined as input and output signals, respectively, the transfer function (TF) which defines the response of $\Theta(t,\ 1)$ to β is

$$G(s,\ 1) = \frac{\hat{\Theta}(s,\ 1)}{\hat{\beta}(s)} = \frac{-\tanh(\sqrt{Ks})}{\tanh(\sqrt{Ks}) - \sqrt{Ks}}, \tag{42}$$

where $\hat{\beta}(s)$ and $\hat{\Theta}(s,1)$ are the Laplace transformations of $\beta(t)$ and $\Theta(t,1)$ (see [30,35]).

Transfer function $G(s,1)$ is also understood as the impulse response of $\hat{\Theta}(s,1)$ and its modal expansion results in the infinite series

$$G(s,1) = K\left(\frac{3}{s} + 2\sum_{m=2}^{\infty}\frac{1}{s-p_m}\right), \tag{43}$$

whose poles p_m are defined above. This expression shows that modes related to nonzero poles are equally important and no truncation criteria could be established from the impulse response. Applying the input pulse (38), with Laplace transformation

$$\hat{\beta}(s) = \frac{1}{s}\left(1 - \mathrm{e}^{-ds}\right), \tag{44}$$

the expansion of the convolution between $G(s,1)$ and $\hat{\beta}(s)$ is

$$G(s,1)\hat{\beta}(s) = K\left[\frac{3}{s^2} + 2\sum_{m=2}^{\infty}\frac{1}{p_m}\left(\frac{1}{s-p_m} - \frac{1}{s}\right)\right]\left(1 - \mathrm{e}^{-ds}\right). \tag{45}$$

In this case, each mode is weighted by a residue $\mathrm{res}_m = 2K/p_m$, which decays as its associated mode becomes faster. This fact allows to define a truncation criteria. Clearly, the most important mode related to a nonzero pole is the second ($m=2$). Then, the order of the approximation in (14) could be selected such that

$$\left|\frac{\mathrm{res}_q}{\mathrm{res}_2}\right| = \left|\frac{p_2}{p_q}\right| = \frac{\lambda_2^2}{\lambda_q^2} \leq \varepsilon, \tag{46}$$

where $\varepsilon \ll 1$ is an arbitrary parameter that could be interpreted as an error measurement.

Moreover, if an oscillating input $\beta(t) = \sin(\omega_0 t)$ is chosen, the expanded response results as

$$G(s,1)\hat{\beta}(s) = K\left(\frac{3}{\omega_0 s} + 2\sum_{m=2}^{\infty}\frac{\omega_0}{\omega_0^2 + p_m^2}\frac{1}{s-p_m} + \frac{b_0 s + c_0}{s^2 + \omega_0^2}\right), \tag{47}$$

where coefficients

$$b_0 = \frac{-3}{\omega_0} - 2\sum_{m=2}^{\infty}\frac{\omega_0}{\omega_0^2 + p_m^2} \quad \text{and} \quad c_0 = -2\sum_{m=2}^{\infty}\frac{p_m}{\omega_0^2 + p_m^2} \tag{48}$$

define the steady-state response. In this case, residues $\mathrm{res}_m = 2K\omega_0/(\omega_0^2 + p_m^2)$ are also functions of frequency ω_0 and take their maximum value $\overline{\mathrm{res}}_m = 2K/|p_m|$ at $\omega_0 = |p_m|$. Then, criterion (46) can be formulated taking the maximum residues $\overline{\mathrm{res}}_m$:

$$\left|\frac{\overline{\mathrm{res}}_q}{\overline{\mathrm{res}}_2}\right| = \left|\frac{p_2}{p_q}\right| = \frac{\lambda_2^2}{\lambda_q^2} \leq \varepsilon. \tag{49}$$

In this case, the response is negligible whether $\omega_0 \gg |p_q|$. When the pulse (38) is considered as an infinite sum of oscillating functions, interpretation of this last result could be that the response due to components of frequency higher than $|p_q|$ could be neglected.

Based on a modal grouping of an expansion similar to (45), obtained for a unit step input signal, a low order and large bandwidth transfer function approximated to (42) was synthesized in [30]. In contrast, expansions (43), (45) and (47) are used in this paper to show that simple residue analysis could brought a practical order selection criterion for the discretized state equations. It should be shown later that reasonably results are straightforward obtained without further alterations of the semidiscretization approximations, as could be suggested by the residue grouping method.

6. Other approximations

Whereas spatial semidiscretization is a very general approach, most of reduced order approximations reported in the literature for the solid phase diffusion problem (1) and (2) are valid just under constant charge or discharge input currents. For instance, an expression based on the Dunhamel's superposition integral, valid either for short or long periods of operation, is proposed in [16,47] to obtain more efficiently numerical solutions of the whole electrochemical model. Simple approximations adjusted to the analytic solution are presented in [35,48], also for short time and steady-state predictions. In [17,25] an equation representing the steady-state solution is used to analyze the solid phase diffusion limitations and determine the capacity of a cell.

For time varying input rates, two dynamic approximations based on low order polynomials are presented and explicitly solved for some input profiles in [27]. For the first, it is assumed that lithium concentration c can be described by a second order polynomial in r of form $c(r,t) = a(t) + b(t)(r/R)^2$. Solving for weights $a(t)$ and $b(t)$ results

$$\begin{aligned}\frac{\mathrm{d}\bar{c}}{\mathrm{d}t} &= \frac{-3}{R}j_n \\ c|_{r=R} &= \bar{c} - \frac{R}{5D}j_n,\end{aligned} \tag{50}$$

which is a first order approximation and just keeps the dynamics associated to the average lithium concentration $\bar{c}$ inside a spheric particle.

Taking the fourth order polynomial $c(r,t) = a(t) + b(t)(r/R)^2 + d(t)(r/R)^4$ and now solving for $a(t)$, $b(t)$ and $d(t)$ results the second order approximation

$$\begin{aligned}\frac{\mathrm{d}\bar{c}}{\mathrm{d}t} &= \frac{-3}{R}j_n \\ \frac{\mathrm{d}\bar{q}}{\mathrm{d}t} &= \frac{-30D}{R^2}\bar{q} - \frac{45}{2R^2}j_n \\ c|_{r=R} &= \bar{c} - \frac{8R}{35D}\bar{q} - \frac{R}{35D}j_n,\end{aligned} \tag{51}$$

where $\bar{q}$ is the volume-averaged concentration flux, which defines the average change of concentration $c(t,r)$ with respect to the position r. $\bar{q}$ is calculated by integrating of $\partial c/\partial r$ along r on the domain $r \in [0, R]$ (see [27] for more details). This approach is applied to the single-particle model for estimation of the state-of-charge in [38,40], state-of-health in [28] and for validation of reduced order models through numerical simulations in [20,31,33]. Because of their recurrent appearance in the literature, (50) and (51) are also tested and compared with the semidiscretization approximations described above.

Some other approximations have been proposed in the frequency domain. In [29] the exact transfer function from $J_n(s)$ to $C(s,R)$, the ratio of the Laplace transformations of $j_n(t)$ and $c(t,R) = c|_{r=R}$, is approximated through a lumped transfer function whose order is arbitrarily proposed with poles optimally found for a certain bandwidth. A similar approach is developed in [30] although, in this case, poles are found by grouping in frequency belts the residues associated to a unit step input and taking the weighted average of their amplitude.

7. Results and discussion

7.1. Order selection

Truncation criteria brought contrasting results. The first criterion is too conservative and drives to relative high order approximations; in this case *order* means the number of ordinary differential equations resulting in the approximations. For the negative electrode results that, according to (41), $\lambda_{n,q}^2 \geq 3141.6$ and the

first value which accomplish that condition is $\lambda^2_{n,19} = 3375.9$. Similar results are obtained for the positive electrode. In this case $\lambda^2_{p,q} \geq 1696.5$ and then $\lambda^2_{p,14} = 1796.7$. In summary, the negative electrode subsystem results of order $q_n = 19$ whereas, for the positive electrode, the subsystem is of order $q_p = 14$. The whole approximated single-particle electrochemical model is of order $Q = 33$.

The plot of normalized residues $|\text{res}_{p,m}/\text{res}_{p,2}| = \lambda^2_2/\lambda^2_m$ of expansion (45) against the index m is shown in Fig. 5. Defining arbitrarily $\varepsilon = 0.05$ in (46) means that amplitude of the residue associated to the faster characteristic value will be 5% the amplitude of that for the slower mode. Taking such value for ε the result is that subsystems of both electrodes would be of order $q_n = q_p = 7$ because $\lambda^2_2/\lambda^2_q = \lambda^2_2/\lambda^2_7 < 0.05$ is held as required in condition (46). Then, the whole approximation is of order $Q = 14$, which is less than half of the order calculated with the bandwidth criterion.

Approximations are first evaluated in the time domain to have a preliminary surmise about which of them has the best trade off between low order and accuracy. In this case, the test signal consists in a rectangular pulse followed by a relaxation time. Then, the frequency response of approximations is compared against that of the analytic transfer function (TF) related to the state equation in order to confirm the results obtained in the time domain tests. Finally, representative cases of all considered approximations are applied to the single-particle model and their response to the HPPC test signal is compared against experimental data extracted from [35].

7.2. Time domain tests

Time was normalized such that $\tau = Kt$, where $K = D/R^2$, and experiments were carried out in the interval $\tau \in [0, 0.45]$. The pulse

$$\beta(\tau) = \begin{cases} 1 & \text{for} \quad \tau \in [0, 0.15) \\ 0 & \text{for} \quad \tau \in [0.15, 0.45] \end{cases} \tag{52}$$

was selected as test signal because it allows the system to reach the steady-state when a constant input is forced, $\beta(\tau) = 1$, as well as during the relaxation stage, $\beta(\tau) = 0$. Programming was carried out with MathWorks® MATLAB®. The base solution was numerically obtained through the *pdepe* routine, which is an initial-boundary value problem solver for parabolic–elliptic partial differential equations (PDEs) in one dimension, based on the algorithm proposed in [49]. The algorithm employed by the solver performs a spatial semidiscretization of parabolic and hyperbolic PDEs by a piecewise nonlinear Galerkin/Petrov–Galerkin method whose truncation

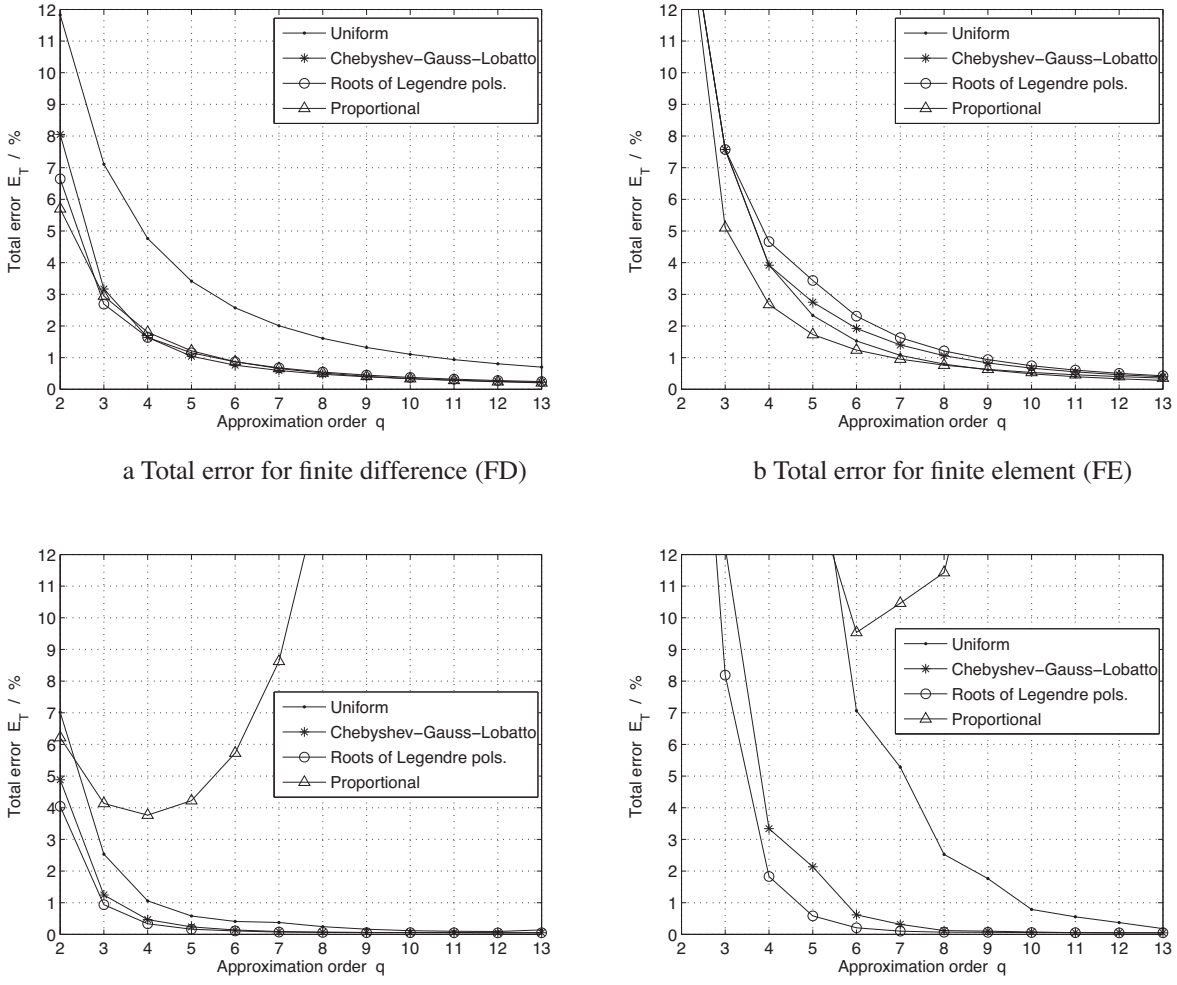

a Total error for finite difference (FD)

b Total error for finite element (FE)

c Total error for polynomial differential quadrature (PDQ)

d Total error for Fourier-based differential quadrature (FDQ)

Fig. 2. Results of tests in the time domain.

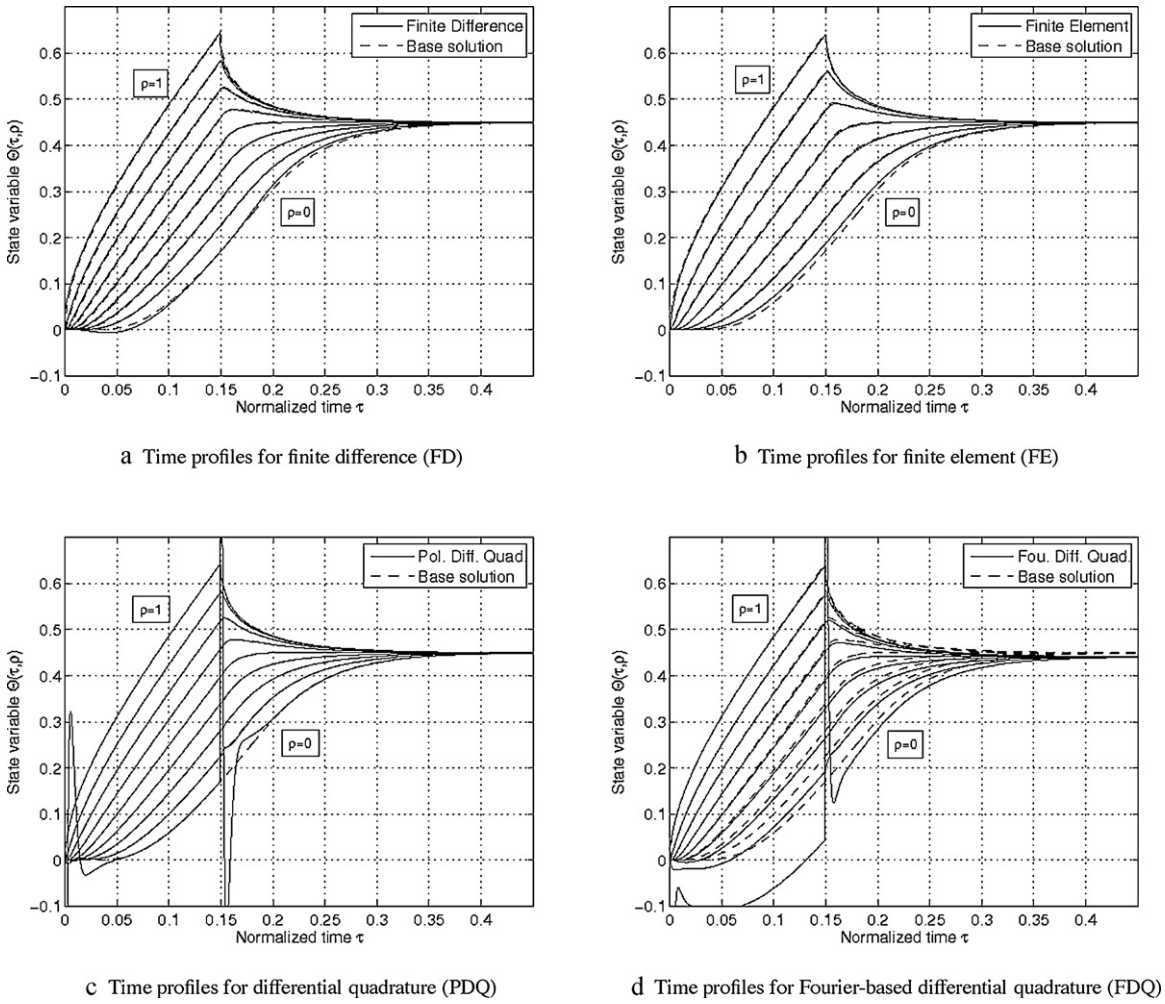

a Time profiles for finite difference (FD)

b Time profiles for finite element (FE)

c Time profiles for differential quadrature (PDQ)

d Time profiles for Fourier-based differential quadrature (FDQ)

Fig. 3. Time profiles for approximations of order $q = 7$ using proportional distribution (PD).

error is of second *order*.[2] A vector of 200 elements uniformly distributed on the space domain was chosen. Time integration, for the base solution and all the approximations, was solved with the *ode15s* routine, a variable order and multistep implicit algorithm for stiff problems, which is based on numerical differentiation (see [50] for more details). Optionally, the solver uses the backward differentiation formulas known as Gear's method. A time vector of 1000 elements evenly separated was specified for the base solution and the approximations. The solver includes a scalar relative error tolerance and a vector of absolute error tolerances for which the default values 1×10^{-3} and 1×10^{-6} were kept, respectively.

Each discretization method was tested along with the four point distributions described in Section 4.4. The total error was individually calculated for each combination using the function

$$E_T = \frac{\mathcal{L}_2\{\boldsymbol{\Theta}_T(t) - \boldsymbol{\Theta}_{base}(t)\}}{\mathcal{L}_2\{\boldsymbol{\Theta}_{base}(t)\}} \times 100\%, \tag{53}$$

where vector $\boldsymbol{\Theta}_T(t)$ is formed by the state vector $\boldsymbol{\Theta}(t)$ and the values of $\Theta_1(t)$ and $\Theta_N(t)$ related to the currently tested approximation, $\boldsymbol{\Theta}_{base}$ results from interpolating the base solution on the corresponding grid and $\mathcal{L}_2\{\circ\}$ implies the Lebesgue 2-norm. Interpolation was carried out with the *pdeval* routine, which approximates the variable $\Theta(t, \rho)$ and its derivative $\partial\Theta(t, \rho)/\partial\rho$ at any specified point using the *pdepe* routine.

Error of approximations evaluated in the time domain are shown in Fig. 2. Excluding the FE method, approximations show their best performance when RLP were used, but similar results are observed for the CGL distribution, which is easier to calculate. In particular, accuracy of PDQ method stands out, even for low order approximations as shown in Fig. 2c. This result is expected as ordinary differential equations resulting from applying the differential quadrature method are strongly coupled. In other words, information from every discretization point is used to infer the value of the state variable at any point of interest. For approximations (50) and (51) based in 2nd and 4th order polynomials, because of no grid is related to these approaches and concentration of Li^+ is of interest just at the surface of representative particles, error was calculated just at $\rho = 1$ resulting of 9.12% and 1.57%, respectively. For the first case, error is too high whereas the second approximation is better than any of the same order.

In general, for all approximations, error E_T decreases whereas order q increases as expected for consistent methods. An exception occurs for PDQ and FDQ when PD is used; in this case, those methods have their worst error. PD produces large errors in $\rho = 0$ an neighboring points as shown in Fig. 3c and d. This phenomenon could be explained because points become more separated and with similar ordinate towards $\rho = 0$. Approximation of spatial derivatives of boundary conditions and state equation lose accuracy, inducing growing errors for high order approximations as shown in Fig. 2c and d. Whether prior knowledge about the spatial profile of state equation exist, it should be a good choice to

[2] In this case *order* is related to the truncation error of the numerical method.

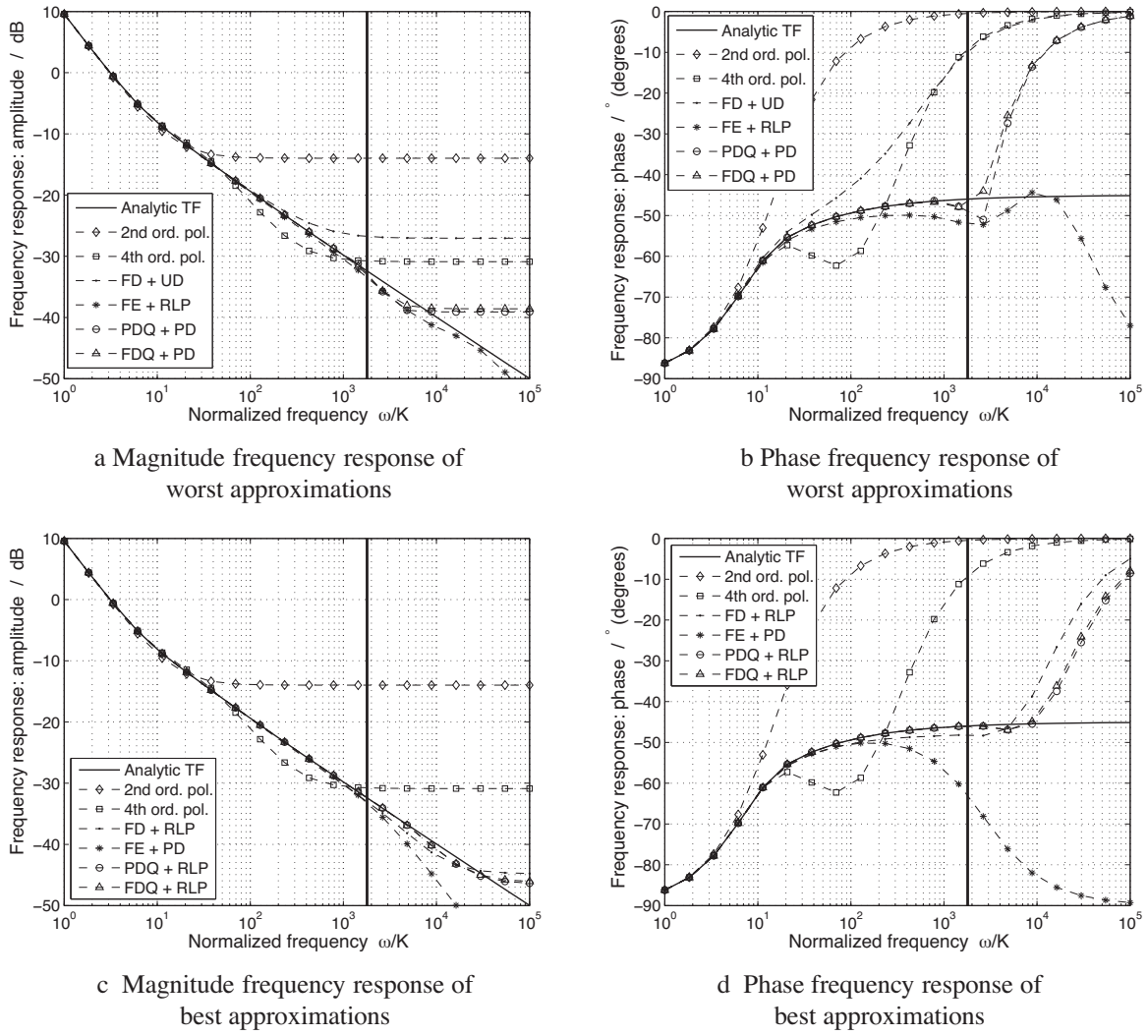

a Magnitude frequency response of worst approximations

b Phase frequency response of worst approximations

c Magnitude frequency response of best approximations

d Phase frequency response of best approximations

Fig. 4. Results of tests in the frequency domain.

tighten up the grid where more pronounced changes are found as suggested in [43]. Thus, PD results to be favorable for FE as shown in Figs. 2b and 3b but does not benefit any other method. On the other hand, the FD method has its worst behavior with UD, used in [39], as shown in Fig. 2a.

7.3. Frequency domain tests

Results discussed so far give a general outlook about the accuracy of different discretization methods along with some grids. However, the test function used is very specific and similar results cannot be ensured in general for different input profiles. Thus, discretization methods were tested also in the frequency domain. In this case, just the best and worst approximations distinguished with the time domain tests were evaluated. Approximations obtained with PDQ and FDQ along to PD, the worst scenario of these methods, were also tested in the frequency domain despite they are unfeasible because error calculated in time domain worsens as order q increases.

Frequency response of magnitude and phase of worst approximations are shown in Fig. 4a and b, whereas responses of best approximations are shown in Fig. 4c and d. In both pairs of figures the base response is that of the analytic TF (42). Responses of approximations (50) and (51), which can also be brought to the general form (14) and (15), are also included in figures. As similar results were observed for higher and lower orders, semidiscretization approximations of order $q = 14$ were arbitrarily selected as examples for frequency response tests (14 is the order for approximations of the positive electrode subsystem when truncation is based on bandwidth selection). Also, in Fig. 4a–d, the vertical bar represents the normalized module of the faster analytic pole p_q of approximations, mentioned in Section 5 and, according to (40), in this case is $|p_{14}/K| = \lambda_{14}^2 = 1796.7$. For more generality, the normalized frequency $\bar{\omega} = \omega/K$ is defined.

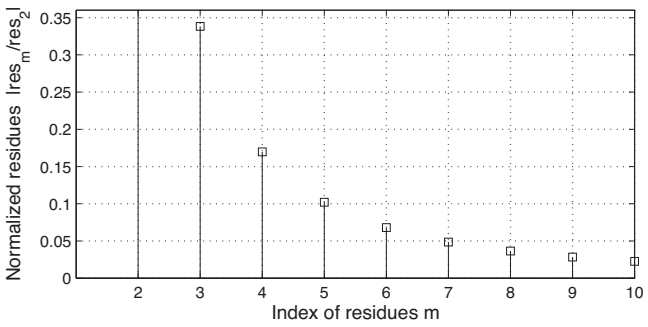

Fig. 5. Normalized residues associated to the pulsating input signal β.

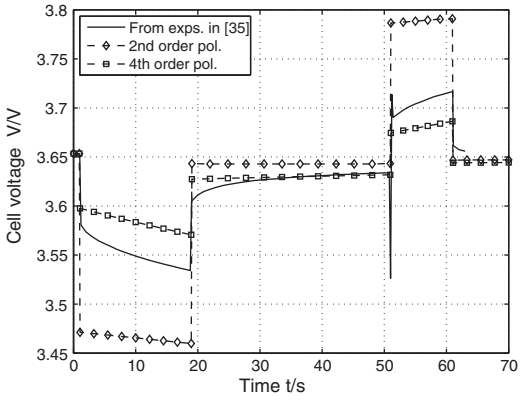

a Cell voltage using low-order polynomial-based approximations

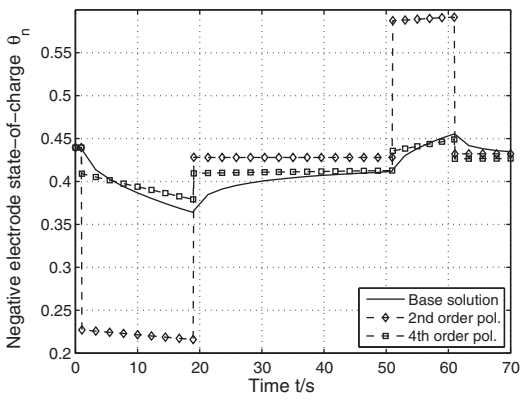

b Negative electrode state-of-charge using low-order polynomial-based approximations

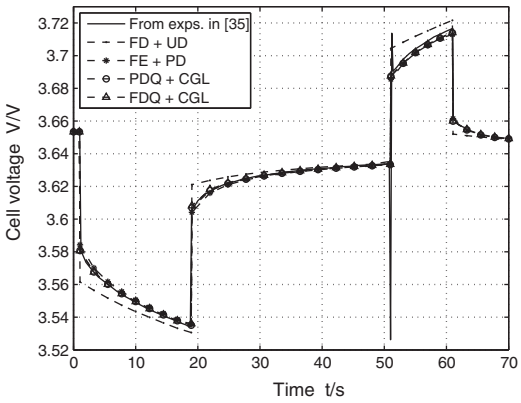

c Cell voltage using semidiscretization approximations and truncation by bandwidth selection

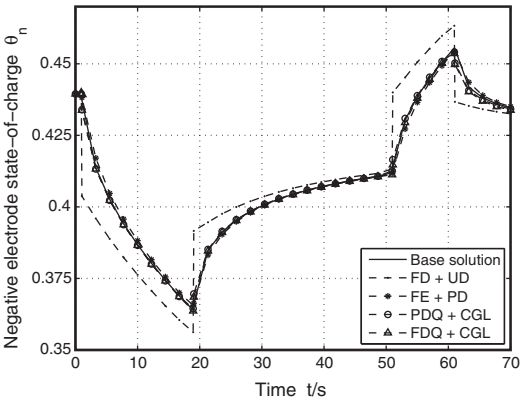

d Negative electrode state-of-charge using semidiscretization approximations and truncation by bandwidth selection

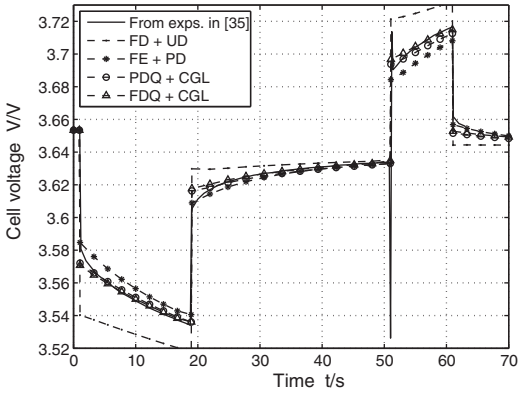

e Cell voltage using semidiscretization approximations and truncation 26 by residue analysis

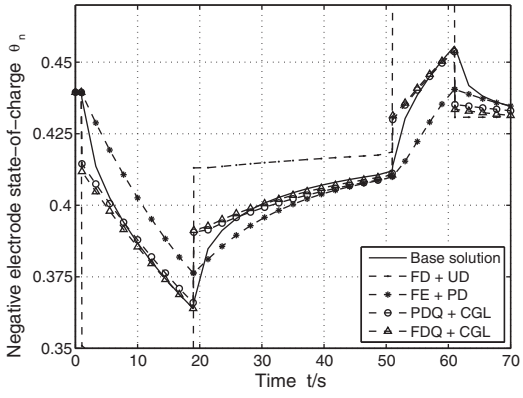

f Negative electrode state-of-charge using semidiscretization approximations and truncation by residue analysis

Fig. 6. Results of test applying the HPPC current profile.

Because of their low order, approximations (50) and (51) have poor but reasonable responses. Particularly, the magnitude response of (51), used in [33], is almost as good as that of the FD 14th-order approximations when using UD. However, the phase responses of (50) and (51) shows the limitations of such approximations, being valid for low frequencies in the interval of $\bar{\omega} \in [0, 10]$.

The worst approximations (see Fig. 4a and b) of PDQ and FDQ showed to have similar magnitude responses, better to that attached to FD and FE despite their growing error obtained in the time tests. PDQ and FDQ approximations sustain a good agreement with the magnitude base response until half decade after $\bar{\omega} = \lambda_{14}^2$ and FD moves away almost one decade before reaching λ_{14}^2. On the other hand, the phase responses of FD diverge too early from the base response and that of PDQ and FDQ keep their agreement to the base phase response until λ_{14}^2. Paradoxically, RLP distribution gives the worst performance to FE in the time domain, but causes its best frequency response.

On the other hand, in Fig. 4c and d, it is shown that the response of semidiscretization approximations improves when using the grids which also drove to the best results in the time domain. PDQ and FDQ magnitude response is close to the base response up to one decade after λ_{14}^2 and half decade for phase response. It should be highlighted that behavior of FD improves when using RLP to the extent that such approximations is almost as good as PDQ in both time and frequency domains. However, for FE the result is opposite again; the frequency response worsens with PD.

7.4. Test with the HPPC signal

The response to the HPPC signal of the single-particle electrochemical model is presented. The voltage evolution of approximations against the response profile reported in [35] for 58.3% of battery SOC, acquired from experimental tests in the same work, is shown. For tests, initial SOC was slightly adjusted to 57% as well as R_f from 20 to 23 $\Omega\,cm^2$. The pair of fast peaks at 52 s was not induced because of the lack of information about them. Nevertheless, due to the sluggish nature of the system, their influence to the cell response is not substantial. The evolution of negative electrode state-of-charge θ_n is also shown as, for this electrode, results from truncation criteria are more drastic. In this case, the base solution was solved numerically using the *pdepe* routine introduced above. Fig. 6a and b correspond to cell response when approximations (50) and (51) are applied. It is reported in the literature that those approximations work well for constant long time and low input current regimes (see for example [20,28]) but, as shown, fail dramatically for pulsating profiles due to their poor bandwidth and thus is not advisable to use this approach for complicated input signals.

For spatial semidiscretization approximations, the most typical grid was considered for each case. UD is used for FD as in [39]. PD is used for FE, which is similar to the grid used in [35]. Finally, CGL is used along with PDQ and FDQ as recommended in [44]. The response of approximations is quite good when model order is chosen by bandwidth selection. Voltage evolution of approximations is shown in Fig. 6c. Approximations related to FE, PDQ and FDQ methods follow very closely the experimental data taken from [35]. In particular, PDQ and FDQ are better than FE and seem to have both the same good accuracy. However, FD used along with UD as reported in the literature, produces a noticeable error because it is the worst grid choice for that method. Nevertheless, as discussed before, the error of FD can be improved whether RLP and CGL grids are used instead of UD. In Fig. 6d, error of approximations is more evident than in Fig. 6c because in the latter case θ_n is affected by function (A.2) of the negative electrode open circuit potential.

The response of the single-particle model when the order of approximations is chosen through the residue analysis is shown in Fig. 6e and f. Voltage responses for PDQ and FDQ seem not to undergo important loss of quality despite the model order is less than half of that obtained by bandwidth selection. Indeed, in this situation, these methods offer a better voltage response than FD when order is defined by bandwidth selection. The response of FE approximation slightly worsens with the order reduction and error of FD increases in a great extent. This is clearer again in the response of negative electrode state-of-charge. Whereas PDQ and FDQ approximations could be still used for state-of-charge estimation, FD and FE approximations are not useful when order is chosen by the second criterion.

8. Conclusions

In this paper the state equation of the single-particle electrochemical model was studied with the goal of finding reduced order approximations that represent adequately the battery main dynamics for some given operation conditions. Spatial semidiscretization approach was reintroduced for order reduction and three discretization methods, combined with four grids, were applied in a classical fashion: finite difference, finite element and differential quadrature. Because of their recurrent appearance in the literature, low order dynamical approximations based on second and fourth order polynomials were also evaluated and compared against semidiscretization approximations. Additionally, two order selection or truncation criteria, suggested but not explored in the literature, were discussed and contrasted. The first, more conservative, consists on selecting the approximation bandwidth such that it covers at least the major part of the energy spectrum of some proposed signal test. The second criterion is based in a residue analysis of the convolution between the state equation and the test signal and drove to more practical results.

Approximations were first evaluated in the time domain to have a preliminary surmise about which had the best trade off between low order and accuracy. In this case, the test signal consisted in a rectangular pulse followed by a relaxation time, whose duration was such that allowed to observe the whole transient response under forced as well as under free excitation. The frequency response of approximations was also compared against that of the analytic transfer function related to the state equation in order to confirm the results obtained in the time domain tests. Finally, representative cases of all considered approximations were applied to the single-particle model and their response to the HPPC test signal was compared against experimental data extracted from the literature. Best results were obtained with discretizations based on polynomial differential quadrature whereas it was also observed that approximations based on low order polynomials have a very poor performance for pulsating input currents.

Acknowledgements

Research was funded by UNAM-PAPIIT grant IN109080 and CONACYT grant 103640. The first author also acknowledges the scholarship granted by CONACYT.

Table B.1
Values of single-particle model parameters and constants.

Descripion	Symbol	Value
Solid phase Li^+ diffusivity	D_n	$2\times10^{-12}\,cm^2\,s^{-1}$
	D_p	$3.7\times10^{-12}\,cm^2\,s^{-1}$
Representative particle radius	R_n	$1\times10^{-4}\,cm$
	R_p	$1\times10^{-4}\,cm$
Specific contact area [a]	a_n	$17\,400\,cm^{-1}$
	a_p	$15\,000\,cm^{-1}$
Element thickness	δ_n	$50\times10^{-4}\,cm$
	δ_{sep}	$25.4\times10^{-4}\,cm$
	δ_p	$36.4\times10^{-4}\,cm$
Sectional cell area	A	$10\,452\,cm^2$
Film resistance at interphase	R_f	$20\,\Omega\,cm^2$
Effective solution conductivity [a]	κ_n	$10.87\times10^{-3}\,S\,cm^{-1}$
	κ_{sep}	$20.08\times10^{-3}\,S\,cm^{-1}$
	κ_p	$10.77\times10^{-3}\,S\,cm^{-1}$
Maximum Li^+ concentration	c_n^{max}	$16.1\times10^{-3}\,mol\,cm^{-3}$
	c_p^{max}	$23.9\times10^{-3}\,mol\,cm^{-3}$
Exchange current density	$i_{0,n}$	$3.6\times10^{-3}\,A\,cm^{-2}$
	$i_{0,p}$	$2.6\times10^{-3}\,A\,cm^{-2}$
Stoichiometry at 0% SOC	θ_n^0	0.126
	θ_p^0	0.936
Stoichiometry at 100% SOC	θ_n^{100}	0.676
	θ_p^{100}	0.442
Subscripts	n	Negative electrode
	sep	Separator
	p	Positive electrode
Faraday's constant	$\mathcal{F}$	$96\,487\,C\,mol^{-1}$
Ideal gas constant	$\mathcal{R}$	$8.3143\,J\,mol^{-1}\,K^{-1}$
Absolute temperature	$\mathcal{T}$	293.15 K (20 °C)

[a] Calculated from data in [29].

Appendix A. Open circuit potentials

For the positive and negative electrodes, respectively:

$$U_p(\theta_p) = 85.681\theta_p^6 - 375.70\theta_p^5 + 613.89\theta_p^4 - 555.65\theta_p^3 + 281.06\theta_p^2 - 76.648\theta_p + 13.1983 - 0.30987\exp\left(5.657\theta_p^{115}\right) \quad \text{(A.1)}$$

$$U_n(\theta_n) = 8.00229 + 5.0647\theta_n - 12.5780\theta_n^{1/2} - 8.6322\times10^{-4}\theta_n^{-1} + 2.1765\times10^{-5}\theta_n^{3/2} - 0.46016\exp[15.0(0.06-\theta_n)] - 0.55364\exp[-2.4326(\theta_n-0.92)] \quad \text{(A.2)}$$

Appendix B. List of parameters

See Appendix Table B.1

References

[1] P. Hall, E. Bain, Energy Policy 36 (2008) 4352–4355.
[2] I. Hadjispaschalis, A. Poullikas, V. Efthimiou, Renewable and Sustainable Energy Reviews 13 (2009) 1513–1522.
[3] R. Brodd, K. Bullock, R. Leising, R. Middaugh, J. Miller, E. Takeuchi, Journal of the Electrochemical Society 151 (2004) K1–K11.
[4] J.-M. Tarascon, M. Armand, Nature 414 (2001) 359–367.
[5] K. Divya, J. Østegaard, Electric Power Systems Research 79 (2009) 511–520.
[6] R. Nelson, Journal of Power Sources 91 (2000) 2–26.
[7] A. Burke, Proceedings of the IEEE 95 (2007) 806–820.
[8] E. Karden, S. Ploumen, B. Fricke, T. Miller, K. Snyder, Journal of Power Sources 168 (2007) 2–11.
[9] M. Armand, J.-M. Tarascon, Nature 451 (2008) 652–657.
[10] T. Markel, A. Brooker, T. Hendricks, V. Johnson, K. Kelly, B. Kramer, M. O'Keefe, S. Sprik, K. Wipke, Journal of Power Sources 110 (2002) 255–266.
[11] L. Gao, S. Liu, R. Dougal, IEEE Transactions in Components and Packaging Technologies 25 (2002) 495–505.
[12] Y. Hu, S. Yurkovich, Y. Guezennec, B. Yurkovich, Journal of Power Sources 196 (2011) 449–457.
[13] S. Abu-Sharkh, D. Doerffel, Journal of Power Sources 130 (2011) 266–274.
[14] M. Chen, G. Rincón-Mora, IEEE Transactions on Energy Conversion 21 (2006) 504–511.
[15] D. Do, C. Forgez, K. Benkara, G. Friedrich, IEEE Transactions on Vehicular Technology 58 (2009) 3930–3937.
[16] T. Fuller, M. Doyle, J. Newman, Journal of the Electrochemical Society 141 (1994) 1–10.
[17] M. Doyle, J. Newman, A. Gozdz, C. Schmutz, J.-M. Tarascon, Journal of the Electrochemical Society 143 (1996) 1890–1903.
[18] C.-Y. Wang, W. Gu, Journal of the Electrochemical Society 145 (1998) 1890–1903.
[19] K. Smith, C.-Y. Wang, Journal of Power Sources 160 (2006) 662–673.
[20] N. Chaturvedi, R. Klein, J. Chrinstensen, J. Ahmed, A. Kojic, IEEE Control Systems Magazine (2010) 49–68.
[21] W. Gu, C.-Y. Wang, Journal of the Electrochemical Society 147 (2000) 49–68.
[22] I. Ong, J. Newman, Journal of the Electrochemical Society 146 (1999) 4360–4365.
[23] P. Ramadass, B. Haran, P. Gomadam, R. White, B. Popov, Journal of the Electrochemical Society 151 (2004) A196–A203.
[24] G. Sikha, B. Popov, R. White, Journal of the Electrochemical Society 151 (2004) A1104–A1114.
[25] M. Doyle, J. Newman, Journal of Applied Electrochemistry 27 (1997) 846–856.
[26] G. Ning, B. Popov, Journal of the Electrochemical Society 151 (2004) A1584–A1591.
[27] V. Subramanian, V. Diwakar, D. Tapriyal, Journal of the Electrochemical Society 152 (2005) A2002–A2008.
[28] S. Santhanagopalan, Q. Guo, P. Ramadass, R. White, Journal of Power Sources 156 (2006) 620–628.
[29] K. Smith, C. Rahn, C.-Y. Wang, Energy Conversion and Management 48 (2007) 2565–2578.
[30] K. Smith, C. Rahn, C.-Y. Wang, Journal of Dynamic Systems, Measurement and Control 130 (2008), 011012-1–011012-8.
[31] V. Subramanian, V. Boovaragavan, V. Ramadesigan, M. Arabadi, Journal of the Electrochemical Society 156 (2009) A260–A271.
[32] C. Speltino, D. Di Domenico, G. Fiengo, A. Stefanopoulou, Proceedings of the 48th Conference on Decision and Control and 28th Chinese Control Conference, December 16–18, IEEE, Shanghai, PR China, 2009, pp. 3276–3281.
[33] R. Klein, N. Chaturvedi, J. Chrinstensen, J. Ahmed, R. Findeisen, A. Kojic, Proceedings of the American Control Conference, June 30–July 02, IEEE, Baltimore, MD, USA, 2010, pp. 6618–6623.
[34] FreedomCAR Battery Test Manual For Power-Assist Hybrid Electric Vehicles, U.S. Department Of Energy/ID-11069, 2003.
[35] K. Smith, C.-Y. Wang, Journal of Power Sources 161 (2006) 628–639.
[36] J.S. Newman, Electrochemical Systems , 2nd ed., Prentice-Hall, 1991.
[37] B. Haran, B. Popov, R. White, Journal of Power Sources 75 (1998) 56–63.
[38] S. Santhanagopalan, R. White, Journal of Power Sources 161 (2006) 1346–1355.
[39] D. Di Domenico, G. Fiengo, A. Stefanopoulou, Proceedings of the 17th International Conference on Control Applications, September 3–5, IEEE, San Antonio, TX, USA, 2008, pp. 702–707.
[40] S. Santhanagopalan, R. White, International Journal of Energy Research 34 (2010) 152–163.
[41] H. Lomax, T.H. Pulliam, D.W. Zingg, Fundamentals of Computational Fluid Dynamics , NASA (electronic publication), 1999.
[42] J. Ferziger, M. Perić, Computational Methods for Fluid Dynamics , Springer, 2002.
[43] J.L. Segerlind, Applied Finite Element Analysis , John Wiley and Sons, 1984.
[44] C. Shu, Differential Quadrature and its Application in Engineering , Springer, 2000.
[45] T. Fung, International Journal for Numerical Methods in Engineering 56 (2003) 405–432.
[46] R. Haberman, Elementary Applied Partial Differential Equations with Fourier Series and Boundary Value Problems , 2nd ed., Prentice Hall, 1987.
[47] M. Doyle, T. Fuller, J. Newman, Journal of the Electrochemical Society 140 (1993) 1526–1533.
[48] C.-Y. Wang, V. Srinivasan, Journal of Power Sources 110 (2002) 364–376.
[49] R.D. Skeel, M. Berzins, SIAM Journal on Scientific and Statistical Computing 11 (1990) 1–32.
[50] L.F. Shampine, M.W. Reichelt, SIAM Journal on Scientific Computing 18 (1997) 1–22.